Advanced Pharmaceutical Bulletin

Accepted Manuscript (unedited)

The manuscript will undergo copyediting, typesetting, and review of the resulting proof before it is published in its final form.

Research Article

How to cite this article:
Sarkardeh A, Ardalani R, Salehi H, Ashabi G, Rahimi A, Kianian F, Salmeh E, Adelipour M, Ranjbaran M. Low-dose nano-niosomal dimethyl fumarate modulates oxidative and inflammatory pathways in an amyloid-beta rat model. Advanced Pharmaceutical Bulletin, doi: 10.34172/apb.47501

Low-dose nano-niosomal dimethyl fumarate modulates oxidative and inflammatory pathways in an amyloid-beta rat model

Amir Hasan Sarkardeh[1†], Ramin Ardalani[1,2†], Hossein Salehi[1], Ghorbangol Ashabi[1], Amirabbas Rahimi[3], Farzaneh Kianian[1], Elaheh Salmeh[4], Maryam Adelipour[5], Mina Ranjbaran[1*]

[1] Department of Physiology, School of Medicine, Tehran University of Medical Sciences, Tehran, Iran
[2] Department of Nanobiotechnology, Faculty of Fundamental Sciences, Comprehensive University of the Islamic Revolution, Tehran, Iran
[3] Molecular Medicine Department, Pasteur Institute of Iran, Tehran, Iran
[4] Department of Clinical Sciences, Faculty of Veterinary Medicine, Science and Research Branch, Islamic Azad University, Tehran, Iran
[5] Chemistry Department, Chungnam National University, Daejeon, South Korea

ARTICLE INFO

Keywords:
Alzheimer disease;
Amyloid beta-protein (25-35);
Dimethyl fumarate;
Nanoparticles;
Neuroinflammation;
Nrf2 protein

Article History:
Submitted: June 06, 2026
Revised: August 18, 2026
Accepted: October 15, 2026
ePublished: November 01, 2026

ABSTRACT

Purpose: Effective disease-modifying treatments for Alzheimer's disease remain limited. We examined low-concentration nano-niosomal dimethyl fumarate (N-DMF) in an acute bilateral hippocampal amyloid-β25–35 rat model.
Methods: DMF-loaded niosomes were characterized by electron microscopy, dynamic light scattering, zeta-potential measurement, encapsulation analysis, and in vitro release. Forty adult male Wistar rats were randomly allocated to Sham, Aβ, Aβ+DMF, or Aβ+N-DMF groups (n=10/group). Free DMF was given orally at 25 mg/kg on four alternate days; N-DMF delivered 1.5 mg DMF per rat per administration (approximately 5.0–6.0 mg/kg). Behavioral outcomes, hippocampal oxidative and inflammatory markers (n=6/group), immunoblot endpoints (n=3/group), and qualitative Congo red staining (n=3 in Sham and Aβ groups) were assessed.
Results: The pre-filtration dispersion had a DLS Z-average of 404.6 nm, a polydispersity index of 0.316, a zeta potential of −34.0 mV, and 78.39% encapsulation efficiency. Compared with untreated Aβ-injected rats, N-DMF was associated with higher phospho-Nrf2, NQO1, and SOD activity; lower BACE1, phospho-NF-κB p65, calcineurin A, NFATC1, C1q, C3, MDA, TNF-α, and IL-6; and better performance in the measured behavioral endpoints.
Conclusion: In this acute model, low-concentration N-DMF was associated with molecular, biochemical, and behavioral changes. These findings do not establish improved brain delivery, carrier-specific efficacy, or a causal relationship between Nrf2 signaling and behavioral outcomes.

***Correspondence Author**
Mina Ranjbaran, Email: m-ranjbaran@sina.tums.ac.ir, ORCID: 0000-0003-4791-8911

† These authors contributed equally to this work and share first authorship.

Introduction

Alzheimer disease is the leading cause of dementia and accounts for an estimated 60%–70% of cases worldwide.[1,2] Its clinical and societal burden is increasing, while effective disease-modifying treatments remain limited.[3] Human Alzheimer's disease develops over years and includes amyloid, tau, vascular, inflammatory, and neurodegenerative changes.[4,5] Amyloidogenic cleavage of amyloid precursor protein by β-site amyloid precursor protein-cleaving enzyme 1 (BACE1) and γ-secretase contributes to Aβ production, but this pathway represents only one component of the human disorder.[6]

Aβ can engage microglial pattern-recognition systems and alter calcium-dependent signaling in experimental models.[7-9] Calcineurin-dependent activation of nuclear factor of activated T cells (NFAT) and activation of nuclear factor kappa B (NF-κB) have each been linked to inflammatory gene expression in the diseased brain.[10-12] Complement proteins provide another connection between glial activation and synaptic injury: microglial C1q and astrocyte-associated C3 can promote the recognition and removal of vulnerable synapses in model systems.[13,14] Model-specific findings require cautious interpretation because experimental neurodegeneration models may reproduce a selected phenotype without representing Alzheimer disease as a whole.[15] Brain phagocytosis can likewise be homeostatic or injurious, depending on context.[16] Loss of synaptic function is closely related to cognitive impairment, and behavioral tasks can provide indirect readouts of the affected neural systems.[17]

The transcription factor Nrf2 coordinates cellular responses to electrophilic and oxidative stress.[18] DMF and related fumarates can influence Nrf2-dependent and Nrf2-independent immune pathways.[19,20] Under basal conditions, Keap1-dependent turnover limits Nrf2 abundance; electrophilic modification of Keap1 permits Nrf2 stabilization and transcription of antioxidant-response genes such as NQO1.[21,22] DMF has therefore been studied in neuroinflammatory and neurodegenerative settings.[23] Its established systemic use is accompanied by adverse effects, including flushing and gastrointestinal symptoms.[24] Nrf2 responses also vary with cellular context and disease stage, which argues against interpreting a single phosphoprotein measurement as proof of sustained pathway activation.[25]

Nanocarriers are being explored as a means of modifying drug stability, release, and tissue exposure.[26] Nano-niosomes have also been investigated as carriers for central nervous system delivery.[27,28] However, the potential advantages of a nano-niosomal formulation should not be interpreted as evidence of improved blood-brain barrier transport without direct measurements of drug exposure in plasma and brain. Therefore, in the present study, we evaluated a DMF-loaded niosomal formulation in an acute bilateral hippocampal Aβ25–35 rat model and compared its molecular, biochemical, and behavioral effects with those observed in Aβ-injected control animals and in animals receiving free DMF at a non-dose-equivalent regimen. The assessments included formulation characteristics, Nrf2/NQO1, BACE1, NF-κB, calcineurin/NFATC1, complement proteins, oxidative and inflammatory markers, and three behavioral tasks. The study was exploratory and was not designed to establish pharmacokinetic superiority, enhanced brain delivery, or a causal pathway.

Materials and Methods

Preparation of DMF-loaded niosomes

DMF-loaded niosomes were produced by thin-film hydration. Cholesterol and Span 60 were dissolved in 6 mL chloroform and 3 mL methanol. The solvents were removed under vacuum at 60°C in a rotary evaporator operating at 150 rpm, leaving a thin lipid film. The film was hydrated for 30 min at 60°C with 10 mL phosphate buffer (pH 7.2) containing DMF while stirring at 120 rpm. The dispersion was sonicated for 5 min using 30-s on/30-s off cycles at 30% amplitude under controlled temperature. It was then passed sequentially through

polycarbonate syringe filters with nominal pore sizes of 200 nm and 100 nm before administration. Particle size, PDI, and zeta potential were not remeasured after this filtration step.

Physicochemical characterization

Particle morphology was examined by scanning electron microscopy (MIRA3; TESCAN, Czech Republic) and transmission electron microscopy. Hydrodynamic diameter and polydispersity index (PDI) were measured at 25°C by dynamic light scattering with a Zetasizer equipped with a 633-nm laser. Surface zeta potential was measured on the same instrument. The reported DLS, PDI, and zeta-potential values describe the selected dispersion before sequential filtration. During formulation optimization, the PDI decreased from approximately 0.4 in initial preparations to 0.316 in the selected preparation; batch-level measurements were not retained. No experiments assessed rat-serum stability, protein-corona formation, aggregation in biological media, or route-specific absorption.

Encapsulation efficiency

Free DMF was separated from the niosomal fraction by ultrafiltration. The formulation was centrifuged at 4°C and 4000 ×g for 20 min in an Amicon Ultra-15 filter (30-kDa molecular-weight cutoff). DMF in the filtrate was measured spectrophotometrically at 210 nm. Encapsulation efficiency was calculated as:

$$\text{Encapsulation efficiency (\%)} = \frac{total\ DMF - free\ DMF}{total\ DMF} \times 100$$

In vitro release

Two milliliters of DMF-loaded niosomes, empty niosomes, or free-DMF solution were placed separately in dialysis bags and immersed in 50 mL phosphate-buffered saline (pH 7.4) at 37°C. Samples were collected at 1, 2, 4, 8, 24, 48, and 72 h, and DMF was quantified at 210 nm. Cumulative release was compared between free DMF and N-DMF. The empty formulation was included only as an in vitro control and was not evaluated as an in vivo treatment group.

Animals and ethical approval

Forty adult male Wistar rats (250–300 g) were maintained at 22 ± 2°C under a 12-h light/dark cycle with unrestricted access to standard food and water. The study used males only, and sex-dependent responses were not assessed. Procedures were approved by the Tehran University of Medical Sciences Ethics Committee (IR.TUMS.AEC.1402.202 and IR.TUMS.AEC.1403.051) and were reported as compliant with ARRIVE guidance, EU Directive 2010/63, and the NIH Guide for the Care and Use of Laboratory Animals. Anesthesia for surgery consisted of intraperitoneal ketamine (70 mg/kg) and xylazine (10 mg/kg), with ketorolac (0.86 mg/kg) given as required for analgesia. At the endpoint, rats received ketamine (100 mg/kg) and xylazine (10 mg/kg); after adequate anesthesia was confirmed, they were decapitated and the remains were disposed of according to institutional procedures.

Acute hippocampal Aβ25–35 model

Under anesthesia, bilateral guide cannulae were positioned over the hippocampi using the Paxinos rat brain atlas (anteroposterior −3.3 mm, mediolateral ±2.0 mm, dorsoventral 3.5 mm). Animals recovered for 5 days. Aβ25–35 (5 μg in 2.5 μL per side; Kimia Pajouh Dorsa, Iran) was then injected bilaterally once daily on study days 1–4.[29] This procedure produces an acute peptide-injection injury and does not reproduce the chronic amyloid, tau, vascular, and neurodegenerative features of human Alzheimer disease.

Treatment groups and dosing

Animals were selected for inclusion based on the predefined body-weight range of 250–300 g and assigned to four experimental groups (n=10/group). The allocation of animals to the four experimental groups was performed randomly. Inclusion criteria were adult male Wistar rats weighing 250–300 g and appearing healthy at study entry. No animals were excluded based on behavioral performance or experimental response. The sample size of 10 animals per group was selected based on previous studies and prior experience from our laboratory.

The Sham group received 3 μL dimethyl sulfoxide (DMSO) bilaterally on days 1–4, followed by 1 mL normal saline by gavage on days 11, 13, 15, and 17. The Aβ group received Aβ25–35 as described above and the same saline schedule. The Aβ+DMF group received Aβ25–35 followed by free DMF (Parsian Pharmaceutical Company, Iran) at 25 mg/kg in 1 mL saline by gavage on days 11, 13, 15, and 17.[30] Body weight was used to calculate the amount administered to each rat; at 250–300 g, this corresponded to 6.25–7.50 mg free DMF per administration. Across four administrations, the nominal cumulative exposure was 100 mg/kg.

The Aβ+N-DMF group received Aβ25–35 followed by DMF-loaded niosomes on days 11, 13, 15, and 17. Each administration contained a fixed DMF-equivalent amount of 1.5 mg per rat. Because rats weighed 250–300 g, this corresponded to approximately 5.0–6.0 mg/kg per administration. Across four administrations, each rat received 6 mg DMF in the nanoformulation, corresponding to a nominal cumulative exposure of approximately 20–24 mg/kg.

Behavioral assessment

Behavioral testing included novel-object recognition, passive avoidance, and the Barnes maze. The researchers who conducted the behavioral tasks were different from the researchers who performed model induction and were blinded to group allocation.

Novel-object recognition test

The novel-object recognition task was conducted on days 16–18 in a 40 × 50 cm arena with 50-cm walls. On day 16, each rat explored the empty arena for 10 min. On day 17, two identical objects were placed in separate corners and exploration was recorded for 10 min. On day 18, one familiar object was replaced with a novel object and exploration was again recorded for 10 min. Recognition was summarized using the discrimination index and the discrimination ratio:

$$d_1 = T_{novel} - T_{familiar}$$

$$d_2 = \frac{d_1}{(T_{novel} + T_{familiar})}$$

Passive avoidance

The apparatus contained illuminated and dark compartments separated by a guillotine door. Its grid floor comprised 2-mm stainless-steel rods placed 10 mm apart. On day 16, each rat acclimated for 5 min, was placed in the illuminated compartment, and was allowed to enter the dark compartment. Entry was followed by one scrambled foot shock (0.5 mA, 1500 μs). On day 17, the procedure was repeated without shock; latency to enter the dark compartment was recorded as the retention outcome.

Barnes maze

Spatial performance was assessed on a circular, 100-cm Plexiglas platform containing twenty 10-cm perimeter holes. A dark 20 × 20 cm escape box could be positioned beneath the target hole and connected by a shallow ramp. Day 16 was an adaptation session: each rat explored the maze for 2 min without the escape box. Acquisition training was conducted on days 17–20, with the target hole and escape box in place; animals completed two 2-min trials per day using stable distal visual cues. On day 21, animals completed a 2-min target-retrieval (memory-

retention) trial using the same target location and procedure as during acquisition; the target hole and escape box remained available. A retention session using the same escape-box location and training procedure has been reported in a Barnes-maze study.[31] This session was therefore not a conventional probe trial, in which the escape box is removed. Escape latency and the number of errors (number of non-target holes investigated before the target hole) were recorded. The newly supplied animal-level Barnes workbook contains one latency and one error value for each rat from the day-21 target-retrieval session, but no day or trial identifiers or acquisition values from days 17–20.

Tissue allocation and sampling

After behavioral testing on day 21, the animals were deeply anesthetized and decapitated. The right hippocampus from three rats in each of the Sham and Aβ groups was fixed in 4% formalin; paraffin blocks were prepared 4 days later for Congo red staining. The left hippocampus from all animals was rapidly dissected, transferred in liquid nitrogen, and stored at −80°C. All 10 rats per group were included in the behavioral assessments. Six biological samples per group were selected at random for biochemical and cytokine assays, and three biological samples per group were selected at random for immunoblotting. Sample selection was not based on behavioral performance or the apparent response of an individual animal. ELISA measurements for each of the six biological samples were performed in duplicate technical wells. The immunoblot sample size of n=3 represents three different rats per group. No animals or samples were reported as excluded from the analyses.

Immunoblotting

Hippocampal protein was extracted in RIPA buffer and quantified with a Bradford assay kit (DNAbioTech, Iran). Thirty micrograms of protein per sample were separated by SDS-PAGE, transferred to PVDF membranes (Bio-Rad Laboratories, USA), and blocked in 5% skim milk in TBST. Membranes were incubated overnight at 4°C with antibodies to phospho-Nrf2 (Ser40; Biorbyt, 1 µg/mL, orb6544), NQO1 (Abcam, 1:10,000, ab80588), BACE1 (Abcam, 1:1000, ab183612), calcineurin A (Abcam, 1:1000, ab282104), NFATC1 (Proteintech, 1:5000, 66963-1-Ig), phospho-NF-κB p65 (Ser536; Abcam, 1:1000, ab76302), C1q (Sigma-Aldrich, 1:10,000, ZRB2039), C3 (Novus Biologicals, 1:1000, NBP1-32080), or β-actin (Abcam, 1:2500, ab8227). HRP-conjugated goat anti-rabbit (Abcam, 1:10,000, ab6721) or goat anti-mouse (Abcam, 1:10,000, ab97240) secondary antibody was used as appropriate. Bands were detected by enhanced chemiluminescence and quantified in ImageJ. Target signals were normalized to β-actin. Three biological samples per group were analyzed; this small sample provides limited precision for pathway-level comparisons.

Congo red staining

Congo red staining was used to qualitatively examine Congo red-positive changes in hippocampal tissue following intrahippocampal administration of Aβ25–35. For this analysis, the right hippocampus from three animals in each of the Sham and Aβ groups was fixed in 4% formalin. After four days, the tissues were processed and embedded in paraffin, and sections were prepared for Congo red staining. The sections were deparaffinized and hydrated and then stained with 1% Congo red solution for 5 min. They were differentiated in potassium hydroxide solution for 3–10 s and rinsed with running water. Hematoxylin was used for nuclear counterstaining. The sections were then dehydrated through graded alcohols, mounted, and examined under a light microscope. The assessment was qualitative; no counting or semiquantitative scoring was performed, and the histological assessment was performed under blinded conditions.

Oxidative-stress and cytokine assays

Malondialdehyde (MDA), used as an index of lipid peroxidation, was measured through its thiobarbituric-acid reaction and absorbance at 532 nm.[32] For superoxide dismutase (SOD), 50 mg hippocampal tissue was

homogenized in 500 µL lysis buffer and centrifuged at 12,000 ×g for 5 min at 4°C. SOD activity was determined at 405 nm with a colorimetric kit (Navand Salamat, Iran) and expressed as reported in the source dataset. Hippocampal TNF-α and IL-6 were measured in duplicate with rat sandwich ELISA kits (Cusabio, China; CSB-E11987r and CSB-E04640r). Optical density was read at 450 nm with 570-nm correction on a BioTek ELX800 plate reader, and concentrations were derived from standard curves.

Statistical analysis

Analyses were performed in GraphPad Prism 10. Values are presented as mean ± SEM. Each endpoint was analyzed separately by one-way ANOVA followed by Tukey's multiple-comparison test, with $P<0.05$ as the significance threshold. For each endpoint, the omnibus F statistic, P value, and omega-squared (ω^2) are reported; Tukey-adjusted P values and Hedges' g are provided for the indicated pairwise comparisons. For the Barnes-maze outcomes, the newly supplied workbook contained one day-21 latency and error value per animal (n=10/group) and no repeated day or trial observations. The day-21 endpoints were therefore analyzed by one-way ANOVA as described above; a repeated-measures or mixed-effects analysis of acquisition across days or trials, including a group-by-time interaction, could not be performed. No primary outcome was prespecified, and no multiplicity adjustment was applied across the different endpoint families. The analyses were therefore considered exploratory, and the findings were interpreted accordingly.

The overall experimental timeline, group assignments, treatment schedule, behavioral assessments, and terminal tissue allocation are summarized in Figure 1.

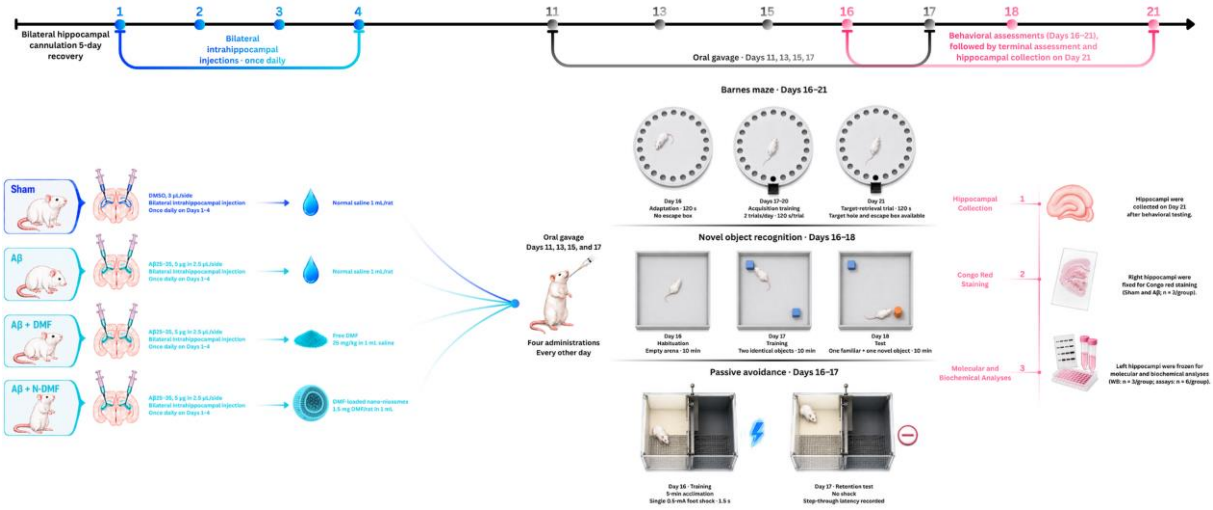


Figure 1. Experimental design and study timeline. After bilateral hippocampal cannulation and a 5-day recovery period, rats received bilateral DMSO or Aβ25–35 injections on study days 1–4 and were assigned to the Sham, Aβ, Aβ+DMF, or Aβ+N-DMF groups (n=10/group). Oral gavage was administered on days 11, 13, 15, and 17. Novel-object recognition was conducted on days 16–18, passive avoidance on days 16–17, and the Barnes maze on days 16–21. After behavioral testing on day 21, hippocampal tissue was collected for qualitative Congo red staining and molecular/biochemical analyses. Aβ, amyloid-β; DMF, dimethyl fumarate; N-DMF, nano-niosomal dimethyl fumarate.

Results

Niosome characterization and DMF release

Electron microscopy showed predominantly rounded vesicular structures. The mean diameter reported from TEM was approximately 380 nm. Before sequential filtration, dynamic light scattering yielded a Z-average of 404.6 nm and a PDI of 0.316, and the measured zeta potential was −34.0 mV (Figure 2a–d). During formulation optimization, the PDI decreased from approximately 0.4 in initial preparations to 0.316 in the selected preparation.

Size, PDI, and zeta potential were not re-evaluated after passage through the 200-nm and 100-nm filters; consequently, the hydrodynamic size and surface charge of the gavaged preparation are unknown. Batch-to-batch PDI, serum stability, protein-corona behavior, aggregation after biological exposure, and route-specific absorption were not measured.

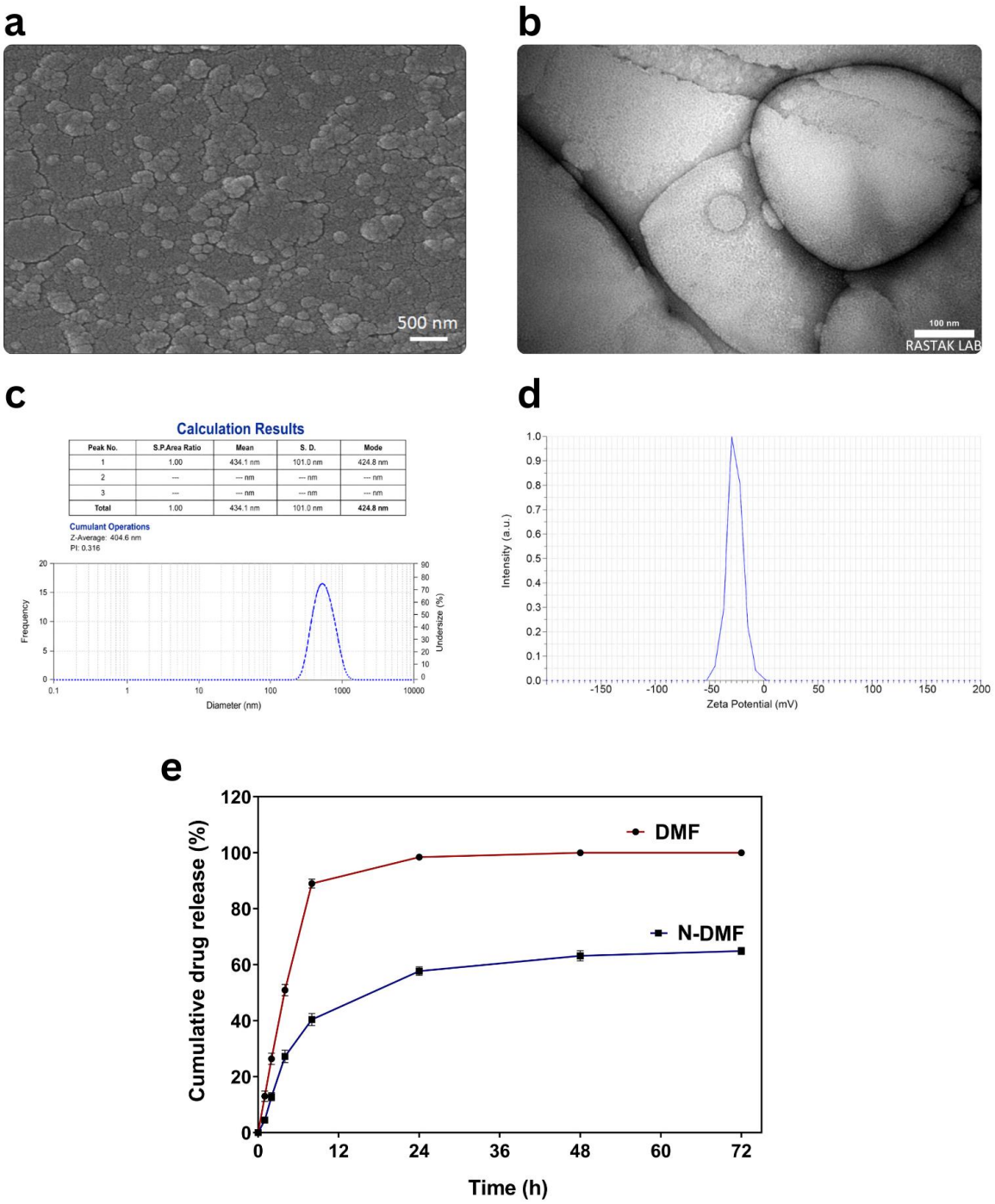


Figure 2. Physicochemical characterization and in vitro release of DMF-loaded niosomes. (a) Scanning electron micrograph. (b) Transmission electron micrograph. (c) Pre-filtration dynamic-light-scattering Z-average and polydispersity index. (d) Pre-filtration surface zeta potential. (e) Dialysis release profiles for free DMF and N-DMF. Points represent the mean ± SEM. Size, PDI, and zeta potential were not remeasured after sequential 200-nm and 100-nm filtration; therefore, these measurements do not establish the physicochemical properties of the gavaged preparation or its behavior in serum or in vivo.

Encapsulation efficiency was 78.39%. Free DMF showed rapid dialysis release, reaching approximately 90% by 10 h and 98.5% by 24 h. N-DMF released 57% at 24 h and 64% at 72 h under the same in vitro conditions (Figure 2e). Among the fitted models, free-DMF release had the highest reported r^2 for the first-order model (0.9287),

whereas N-DMF had the highest r^2 for the Higuchi model (0.8605; Table 1). These in vitro findings describe release under the assay conditions and do not establish route-specific absorption.

Table 1. Release-model fits reported for free DMF and the selected N-DMF formulation.

Release model/parameter	Free DMF	N-DMF
Zero-order (r^2)	0.5253	0.7051
First-order (r^2)	0.9287	0.7900
Higuchi (r^2)	0.6991	0.8605
Korsmeyer–Peppas (r^2)	0.8121	0.8526
Korsmeyer–Peppas (n)	0.4471	0.5676

Nrf2-related proteins

One-way ANOVA showed significant group effects for hippocampal phospho-Nrf2 (Ser40) [$F(3,8)=169.38$, $P<0.0001$, $\omega^2=0.980$] and NQO1 [$F(3,8)=227.74$, $P<0.0001$, $\omega^2=0.983$] (Figure 3). For phospho-Nrf2, Tukey testing showed a lower signal in Aβ than in Sham ($P<0.0001$, Hedges' $g=9.96$) and higher signals in Aβ+DMF ($P=0.0116$, $g=4.66$) and Aβ+N-DMF ($P=0.0006$, $g=7.53$) than in Aβ. The two treatment groups did not differ ($P=0.1122$).

For NQO1, the signal was lower in Aβ than in Sham ($P<0.0001$, Hedges' $g=16.03$) and higher in Aβ+DMF ($P=0.0022$, $g=3.30$) and Aβ+N-DMF ($P<0.0001$, $g=9.30$) than in Aβ. NQO1 was also higher in Aβ+N-DMF than in Aβ+DMF ($P<0.0001$, $g=6.93$; Figure 3). These analyses were based on n=3 biological samples/group.

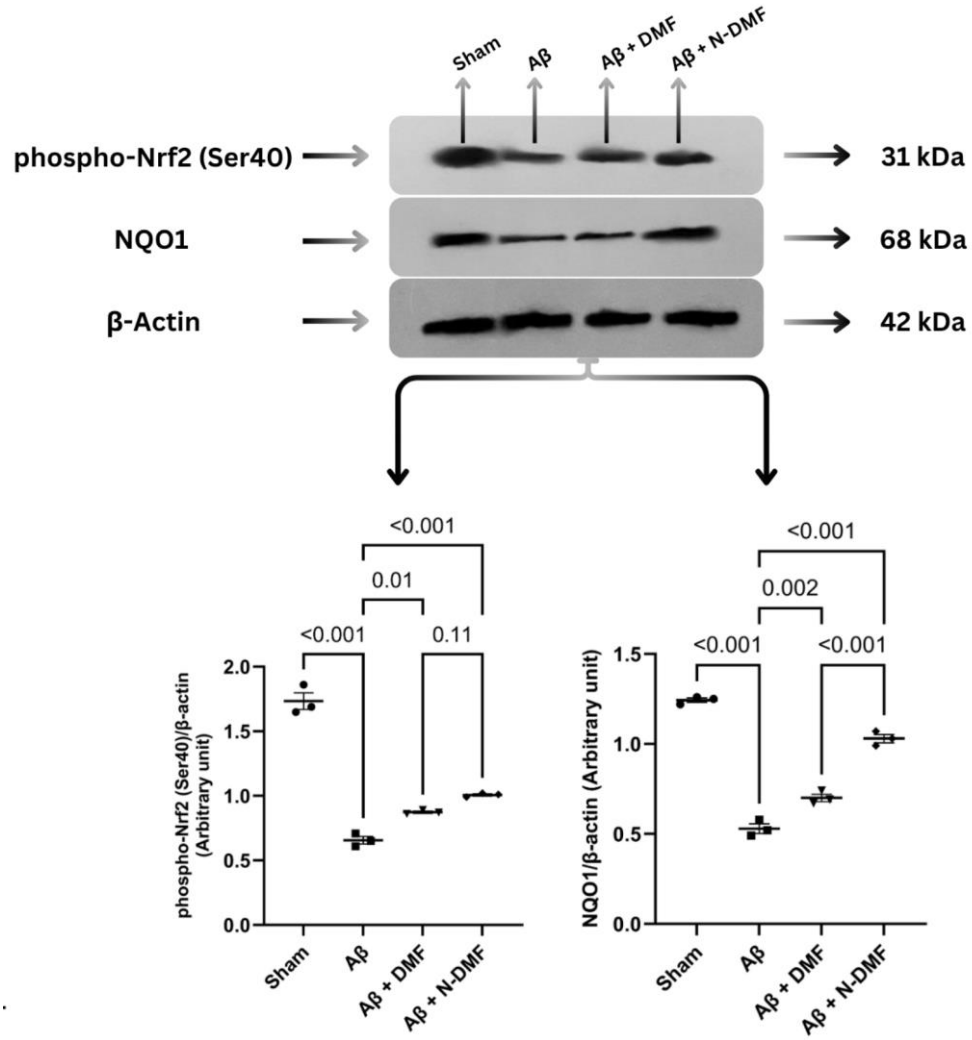


Figure 3. Hippocampal phospho-Nrf2 and NQO1 after treatment. Representative immunoblots and densitometric summaries normalized to β-actin are shown (n=3 biological samples/group). Individual points represent biological samples; horizontal lines and error bars indicate the mean ± SEM. Brackets display Tukey-adjusted P values, rounded in the figure for legibility; the corresponding effect sizes are reported in the Results.

BACE1, NF-κB, calcineurin, and NFATC1

One-way ANOVA showed significant group effects for BACE1 [$F(3,8)=166.45$, $P<0.0001$, $\omega^2=0.976$] and phospho-NF-κB p65 (Ser536) [$F(3,8)=67.31$, $P<0.0001$, $\omega^2=0.943$] (Figure 4a). BACE1 was higher in Aβ than in Sham ($P<0.0001$, Hedges' $g=10.50$) and lower in Aβ+DMF ($P<0.0001$, $g=6.10$) and Aβ+N-DMF ($P<0.0001$, $g=8.58$) than in Aβ; Aβ+N-DMF was also lower than Aβ+DMF ($P=0.0016$, $g=6.99$). Phospho-NF-κB was higher in Aβ than in Sham ($P<0.001$, $g=6.51$) and lower in Aβ+DMF ($P=0.0008$, $g=3.42$) and Aβ+N-DMF ($P<0.001$, $g=5.46$) than in Aβ; Aβ+N-DMF was lower than Aβ+DMF ($P=0.0050$, $g=5.42$).

Significant group effects were also detected for calcineurin A [$F(3,8)=61.84$, $P<0.0001$, $\omega^2=0.938$] and NFATC1 [$F(3,8)=373.58$, $P<0.0001$, $\omega^2=0.989$]. Calcineurin A was higher in Aβ than in Sham ($P<0.0001$, Hedges' $g=7.93$) and lower in Aβ+DMF ($P=0.0009$, $g=5.67$) and Aβ+N-DMF ($P<0.0001$, $g=6.67$) than in Aβ; Aβ+N-DMF was lower than Aβ+DMF ($P=0.0330$, $g=2.45$). NFATC1 was higher in Aβ than in Sham ($P<0.0001$, $g=15.23$) and lower in Aβ+DMF ($P<0.0001$, $g=20.90$) and Aβ+N-DMF ($P<0.0001$, $g=37.01$) than in Aβ; Aβ+N-DMF was lower than Aβ+DMF ($P=0.0001$, $g=12.71$; Figure 4a). These immunoblot analyses used n=3/group and provide limited precision despite the large standardized effects.

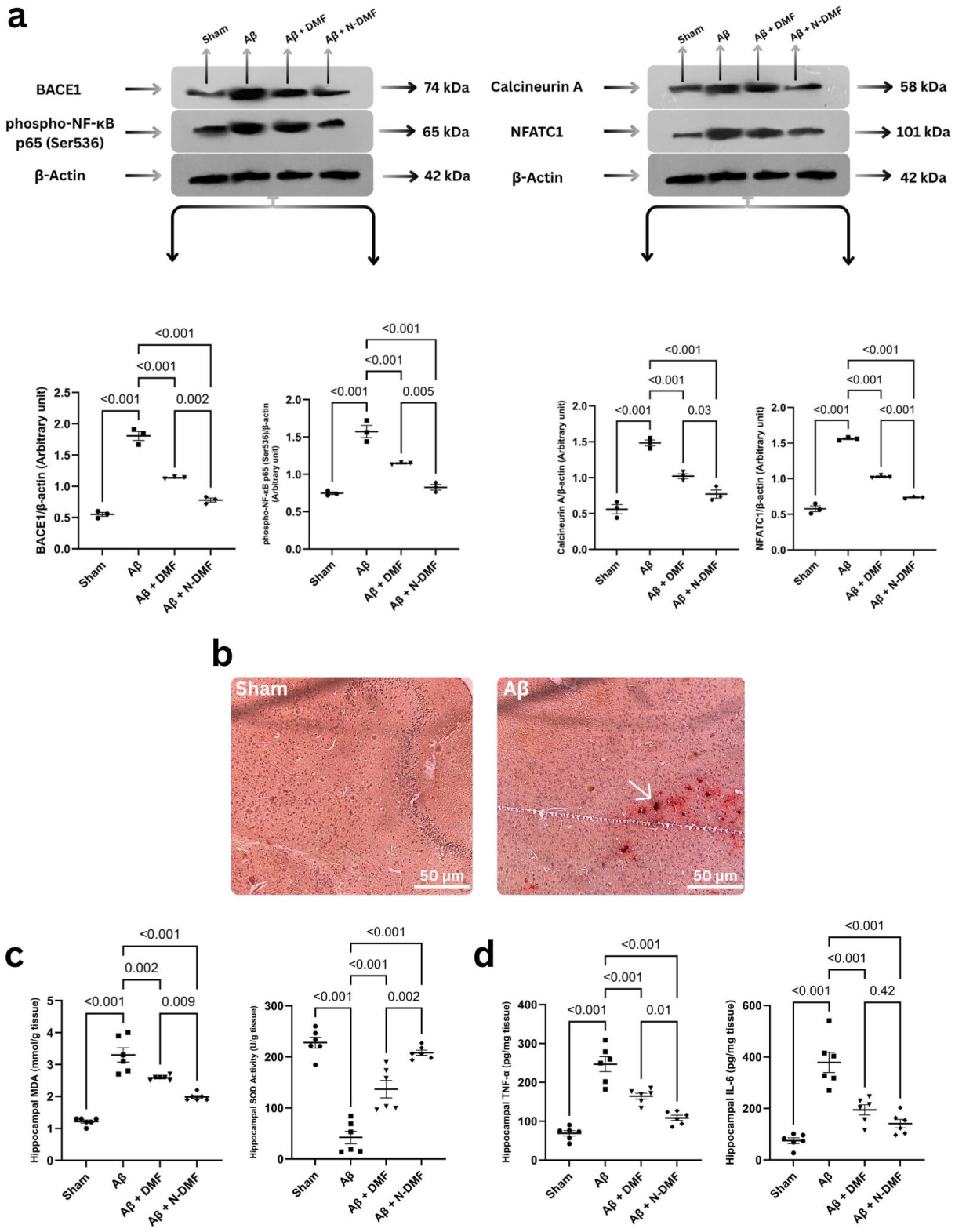


Figure 4. Hippocampal signaling proteins, qualitative Congo red staining, oxidative-stress markers, and inflammatory cytokines. (a) Representative immunoblots and densitometric summaries for BACE1, phospho-NF-κB p65 (Ser536), calcineurin A, and NFATC1, normalized to β-actin (n=3/group). (b) Representative Congo red-stained sections from Sham and Aβ groups (n=3/group); the assessment was qualitative and was not quantitatively scored. (c) Hippocampal MDA and SOD (n=6/group). (d) Hippocampal TNF-α and IL-6 (n=6/group). Individual points in the quantitative panels represent biological samples; horizontal lines and error bars indicate the mean ± SEM. Brackets display Tukey-adjusted P values, rounded in the figure for legibility; the corresponding effect sizes are reported in the Results.

Congo red staining

Congo red staining showed localized red-stained areas in the hippocampal tissue of Aβ25–35-treated rats, whereas similar staining was not observed in the Sham group (Figure 4b). The assessment included three animals per group and was qualitative, with no counting or semiquantitative scoring performed. The Congo red findings were considered qualitative observations and were not interpreted as evidence of amyloid plaques equivalent to those observed in human Alzheimer's disease.

Oxidative and inflammatory markers

One-way ANOVA showed significant group effects for hippocampal MDA [$F(3,20)=56.47$, $P<0.0001$, $\omega^2=0.874$] and SOD activity [$F(3,20)=48.48$, $P<0.0001$, $\omega^2=0.860$] (Figure 4c). MDA was higher in Aβ than in Sham ($P<0.0001$, Hedges' $g=4.86$) and lower in Aβ+DMF ($P=0.0018$, $g=1.69$) and Aβ+N-DMF ($P<0.0001$, $g=3.07$) than in Aβ; Aβ+N-DMF was lower than Aβ+DMF ($P=0.0089$, $g=5.63$). SOD activity was lower in Aβ than in Sham ($P<0.0001$, $g=6.04$) and higher in Aβ+DMF ($P=0.0001$, $g=2.38$) and Aβ+N-DMF ($P<0.0001$, $g=6.58$) than in Aβ; Aβ+N-DMF was higher than Aβ+DMF ($P=0.0023$, $g=2.15$; Figure 4c).

Group effects were also detected for TNF-α [$F(3,20)=45.14$, $P<0.0001$, $\omega^2=0.847$] and IL-6 [$F(3,20)=29.05$, $P<0.0001$, $\omega^2=0.778$] (Figure 4d). TNF-α was higher in Aβ than in Sham ($P<0.0001$, Hedges' $g=4.61$) and lower in Aβ+DMF ($P=0.0003$, $g=2.11$) and Aβ+N-DMF ($P<0.0001$, $g=3.59$) than in Aβ; Aβ+N-DMF was lower than Aβ+DMF ($P=0.0127$, $g=2.91$). IL-6 was higher in Aβ than in Sham ($P<0.0001$, $g=3.97$) and lower in Aβ+DMF ($P=0.0002$, $g=2.22$) and Aβ+N-DMF ($P<0.0001$, $g=2.97$) than in Aβ. The two treatment groups did not differ for IL-6 ($P=0.4206$; Figure 4d).

Complement proteins and behavioral outcomes

One-way ANOVA showed significant group effects for C1q [$F(3,8)=20.05$, $P=0.0004$, $\omega^2=0.826$] and C3 [$F(3,8)=12.35$, $P=0.0023$, $\omega^2=0.739$] (Figure 5a). C1q was higher in Aβ than in Sham ($P=0.0003$, Hedges' $g=3.64$) and lower in Aβ+DMF ($P=0.0117$, $g=2.06$) and Aβ+N-DMF ($P=0.0029$, $g=2.72$) than in Aβ; the treatment groups did not differ ($P=0.6866$). C3 was higher in Aβ than in Sham ($P=0.0023$, $g=2.72$) and lower in Aβ+DMF ($P=0.0359$, $g=1.62$) and Aβ+N-DMF ($P=0.0055$, $g=2.40$) than in Aβ; the treatment groups did not differ ($P=0.5221$; Figure 5a).

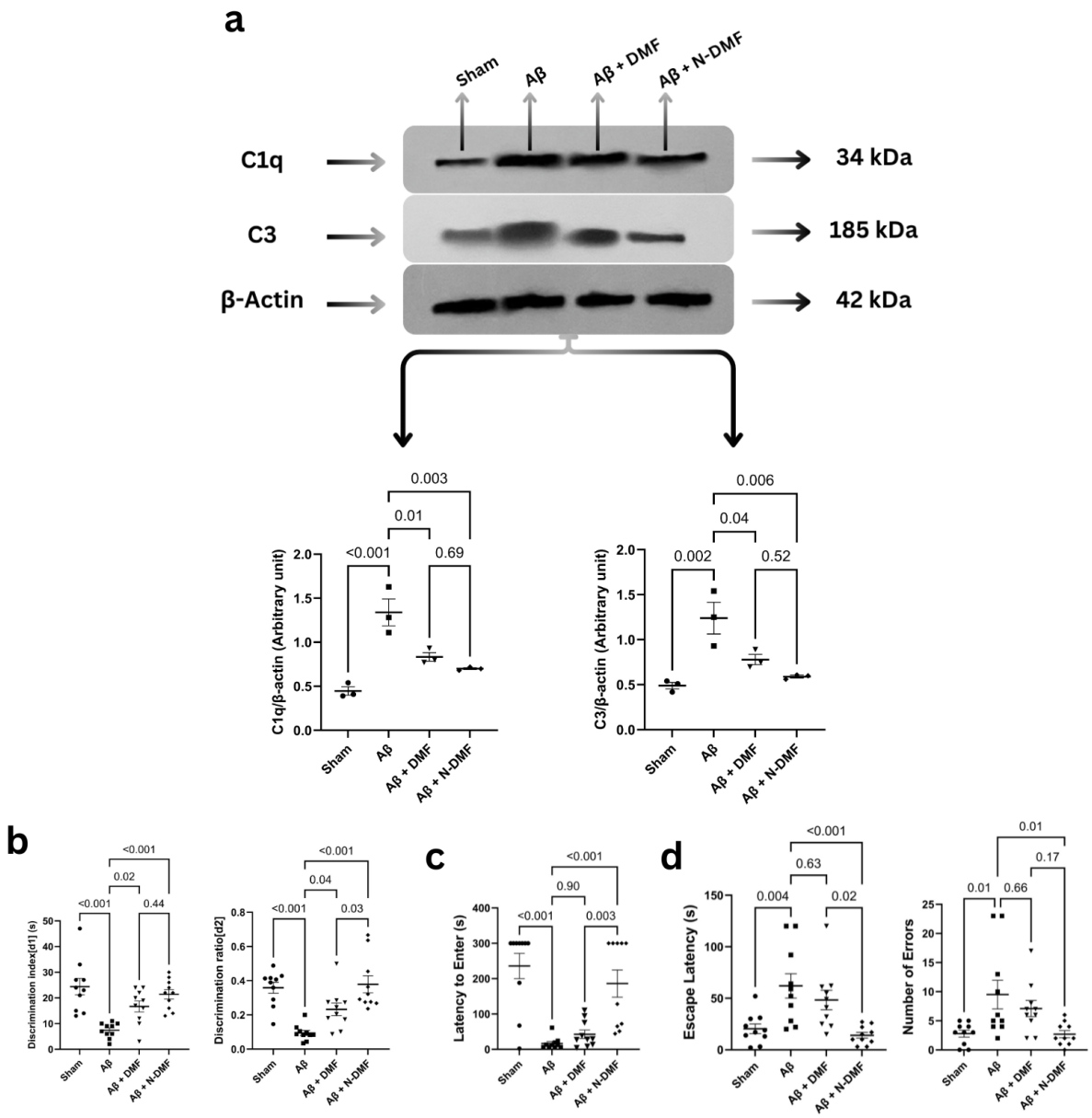


Figure 5. Hippocampal complement proteins and behavioral outcomes. (a) Representative C1q and C3 immunoblots and densitometric summaries normalized to β-actin (n=3/group). (b) Novel-object recognition discrimination index (d1) and ratio (d2; n=10/group). (c) Passive-avoidance retention latency (n=10/group). (d) Day-21 Barnes target-retrieval latency and errors with the target hole and escape box available (n=10/group). Individual points represent biological samples in panel a and individual animals in panels b–d; horizontal lines and error bars indicate the mean ± SEM. Brackets display Tukey-adjusted P values, rounded in the figure for legibility; the corresponding effect sizes are reported in the Results.

For novel-object recognition, one-way ANOVA showed group effects for d1 [$F(3,36)=11.50$, $P<0.0001$, $\omega^2=0.440$] and d2 [$F(3,36)=13.75$, $P<0.0001$, $\omega^2=0.489$] (Figure 5b). For d1, Aβ was lower than Sham ($P<0.001$, Hedges' $g=2.17$), whereas Aβ+DMF ($P=0.0200$, $g=1.72$) and Aβ+N-DMF ($P<0.001$, $g=2.91$) were higher than Aβ; the treatment groups did not differ ($P=0.44$). For d2, Aβ was lower than Sham ($P<0.001$, $g=3.22$), whereas Aβ+DMF ($P=0.0432$, $g=1.50$) and Aβ+N-DMF ($P<0.001$, $g=2.37$) were higher than Aβ. Aβ+N-DMF was also higher than Aβ+DMF ($P=0.0296$, $g=1.02$; Figure 5b).

Passive-avoidance retention latency differed among groups [$F(3,36)=15.68$, $P<0.0001$, $\omega^2=0.524$]. Latency was shorter in Aβ than in Sham ($P<0.0001$, Hedges' $g=2.61$) (Figure 5c). Aβ+DMF did not differ from Aβ ($P=0.90$) and remained lower than Sham ($P=0.0001$, $g=2.20$). Aβ+N-DMF had a longer latency than Aβ ($P=0.0005$, $g=1.86$) and Aβ+DMF ($P=0.0034$, $g=1.52$; Figure 5c).

On the day-21 Barnes target-retrieval trial, group effects were detected for escape latency [$F(3,36) = 7.94$, $P = 0.000343$, $\omega^2 = 0.342$] and number of errors [$F(3,36) = 5.15$, $P = 0.004584$, $\omega^2 = 0.237$] (Figure 5d). Latency was longer in Aβ than in Sham ($P = 0.004433$, Hedges' $g = 1.40$) and shorter in Aβ+N-DMF than in Aβ ($P = 0.000928$, $g = 1.69$) and Aβ+DMF ($P = 0.02420$, $g = 1.48$); Aβ+DMF did not differ from Aβ ($P = 0.6303$). Aβ made more errors than Sham ($P = 0.01425$, $g = 1.13$), and Aβ+N-DMF made fewer errors than Aβ ($P = 0.01259$, $g = 1.15$). Error counts did not differ between Aβ and Aβ+DMF ($P = 0.6620$) or between the two treatment groups ($P = 0.1703$; Figure 5d). The supplied raw values reproduced the individual points and group means shown in Figure 5d. These values represent a single target-retrieval session conducted with the target hole and escape box available; they are not probe-trial outcomes or longitudinal acquisition curves.

Discussion

This exploratory experiment combined formulation measurements with hippocampal protein, biochemical, histologic, and behavioral endpoints in an acute Aβ25–35 injection model. The Aβ group showed lower phospho-Nrf2 and NQO1, higher oxidative and inflammatory markers, altered complement and signaling proteins, and poorer task performance. Both DMF regimens were associated with changes in several of these measures. N-DMF was associated with changes in the measured signaling proteins and behavioral outcomes at a fixed DMF-equivalent amount of 1.5 mg per rat (approximately 5.0–6.0 mg/kg per administration), compared with the 25-mg/kg free-DMF regimen. Because the regimens were not dose-equivalent and systemic or brain exposure was not measured, the study cannot determine whether those differences arose from the carrier, dose, release profile, systemic exposure, brain delivery, or another factor.

The reported 404.6-nm DLS value, PDI of 0.316, and zeta potential of −34.0 mV were obtained before the dispersion was passed sequentially through 200-nm and 100-nm polycarbonate filters. Because size, PDI, and zeta potential were not remeasured after filtration, the physicochemical properties of the gavaged preparation cannot be inferred from the pre-filtration measurements. Sonication and filtration were process steps rather than evidence of biological stability. Rat-serum stability, protein-corona formation, aggregation in biological media, batch-to-batch variability, and route-specific absorption were not assessed and therefore remain uncharacterized.

The in vitro formulation showed sustained release relative to free DMF, but the approximately 400-nm pre-filtration hydrodynamic size is comparatively large for a system described as a CNS nanocarrier. Niosomes can alter drug release and tissue handling,[33] and nanocarriers are under study for brain-directed delivery.[34] Even so, the present work did not measure DMF or monomethyl fumarate in plasma or brain, nor did it directly track the niosomal carrier. Therefore, although N-DMF was associated with changes in several molecular and behavioral outcomes, these findings cannot establish improved brain delivery or enhanced blood-brain barrier transport. Pharmacokinetic and biodistribution studies will be required to determine whether the nano-niosomal formulation alters DMF exposure in the brain.

The MDA and SOD pattern in Aβ-injected animals is consistent with redox disturbance reported in amyloid-related experimental systems.[35] It should nevertheless be distinguished from the multifactorial oxidative pathology of chronic human Alzheimer disease.[36] Nrf2 regulation can vary by disease context, timing, and cell type.[37,38] NF-κB may also compete with Nrf2-dependent transcriptional programs, providing a plausible basis for parallel changes without proving directional mediation.[39] In the present study, phospho-Nrf2 and NQO1 moved in the same direction after treatment, but only a single terminal time point and three immunoblot samples per group were evaluated.

DMF can modify Keap1-associated redox sensing and has broader electrophile-dependent effects.[40,41] The concurrent reductions in phospho-NF-κB p65, TNF-α, and IL-6 are therefore biologically plausible, and NF-κB

has well-described relevance to Alzheimer-related inflammatory signaling.[42] However, the current data are associative. No Nrf2 inhibitor, genetic manipulation, cell-specific measurement, or mediation analysis was used; therefore, the findings do not establish that Nrf2 caused the observed changes in downstream proteins, complement components, or behavioral outcomes.

Calcineurin/NFAT signaling has been associated with cognitive decline and neural stress in Alzheimer-related research.[43] NF-κB can also regulate BACE1 expression in experimental systems.[44] The observed group differences in calcineurin A, NFATC1, phospho-NF-κB, and BACE1 are compatible with these reports, but they neither establish activation within a specific cell type nor show a linear chain from Nrf2 to behavior. Likewise, lower C1q and C3 do not demonstrate preserved synapse number because synaptophysin, PSD-95, microglial engulfment, and direct synaptic measurements were not obtained.

A conceptual summary of the measured associations and proposed, untested relationships is provided in Figure 6.

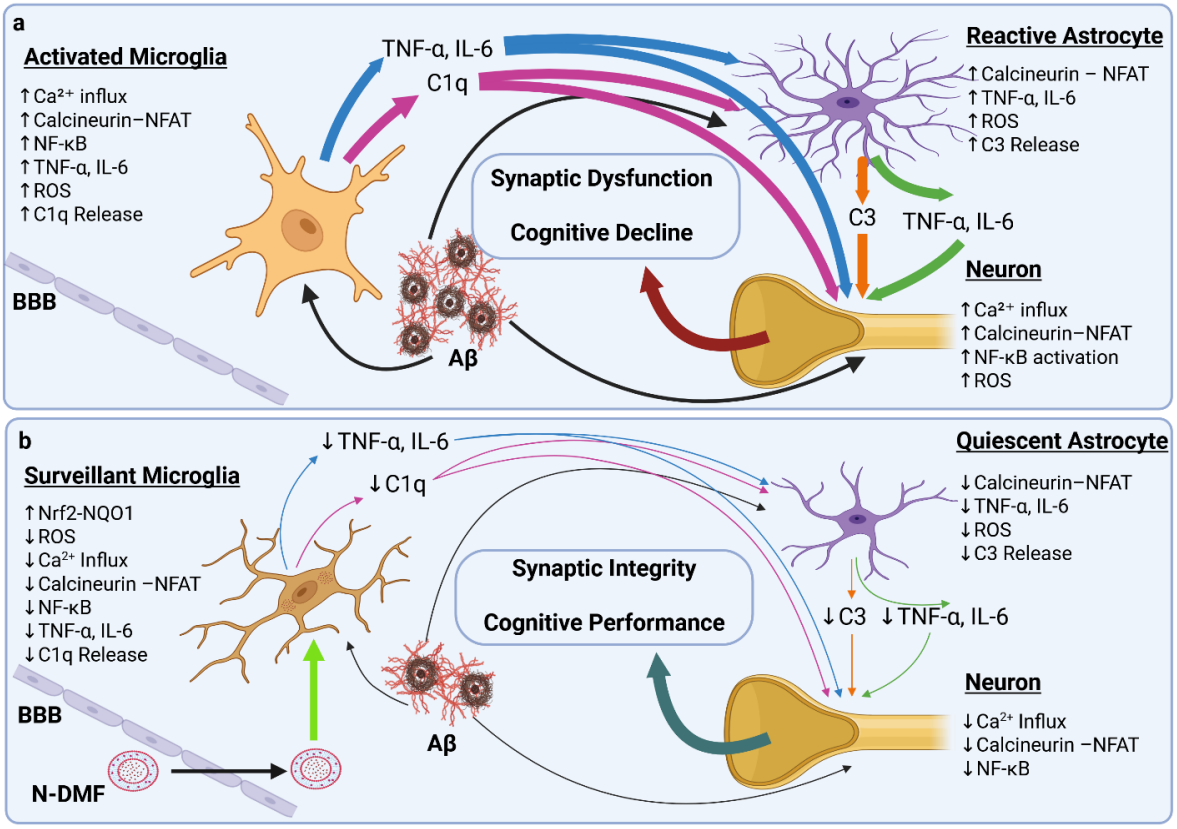


Figure 6. Conceptual summary of the measured associations and proposed neuroinflammatory framework in the acute Aβ25–35 hippocampal-injection rat model. (a) The upper panel depicts Aβ-associated glial and neuronal stress, including calcineurin–NFAT and NF-κB signaling, oxidative and inflammatory mediators, and complement proteins. (b) The lower panel summarizes a proposed interpretation of the group-level changes observed with N-DMF, including higher Nrf2/NQO1, lower MDA, cytokines, and C1q/C3, and better behavioral performance. This schematic is hypothesis-generating: the arrows do not establish a causal sequence, and BBB transport, cell-specific uptake, glial phenotype, synaptic tagging, and synaptic integrity were not directly measured. Abbreviations: Aβ, amyloid-β; BBB, blood–brain barrier; C1q, complement component 1q; C3, complement component 3; DMF, dimethyl fumarate; IL-6, interleukin-6; N-DMF, nano-niosomal dimethyl fumarate; NFAT, nuclear factor of activated T cells; NF-κB, nuclear factor kappa B; NQO1, NAD(P)H quinone dehydrogenase 1; Nrf2, nuclear factor erythroid 2-related factor 2; ROS, reactive oxygen species; TNF-α, tumor necrosis factor-alpha. Created with BioRender.com.

The behavioral interpretation has also been narrowed. Day 16 of the Barnes protocol was adaptation without an escape box. During days 17–20, rats were trained with the target hole and box available. The day-21 session used the same target and box and is therefore described as a target-retrieval trial, not a probe trial. Only one day-21 latency and error value per animal was present in the supplied raw workbook; because days 17–20 and trial identifiers were absent, a group-by-time analysis of acquisition could not be performed.

Several further limitations affect interpretation. The acute hippocampal Aβ25–35 injury does not reproduce chronic amyloid accumulation, tau pathology, vascular disease, or progressive neurodegeneration in humans. Qualitative Congo red staining in three animals per group, without counting or semiquantitative scoring, cannot validate a human-like plaque phenotype. There was no empty-niosomal in vivo group or Sham+N-DMF group, so carrier effects and tolerability cannot be fully separated from DMF effects. Although animals were randomly assigned and behavioral testing was conducted by blinded researchers who were separate from the researchers performing model induction, the exact random-sequence method, allocation concealment, cage-level randomization, and outcome analysis were not recorded. The study also used small assay samples, especially n=3 for immunoblotting; did not prespecify a primary outcome; and did not adjust for multiplicity across endpoint families. The findings are consequently hypothesis-generating and require confirmation with dose-matched controls, adequate power, pharmacokinetics, biodistribution, toxicity assessment, and longitudinal statistics.

Conclusion

In an acute bilateral hippocampal Aβ25–35 rat model, low-concentration N-DMF treatment was associated with changes in Nrf2-related, oxidative, inflammatory, complement, and behavioral measures. As an acute injury model, this paradigm does not reproduce the chronic amyloid, tau, vascular, and neurodegenerative features of human Alzheimer's disease. These findings suggest that low-dose N-DMF may influence multiple molecular and behavioral responses in this model. However, the present study does not establish improved brain delivery, carrier-specific efficacy, or a causal relationship between Nrf2 signaling and behavioral outcomes. Further studies incorporating dose-equivalent free and formulated DMF, appropriate vehicle controls, and pharmacokinetic and biodistribution assessments are warranted to clarify these effects.

Ethical Approval

All experimental procedures were approved by the Tehran University of Medical Sciences Ethics Committee (IR.TUMS.AEC.1402.202 and IR.TUMS.AEC.1403.051) and were conducted under the institutional animal-care framework described in the Methods.

Authors' Contributions

Conceptualization: Mina Ranjbaran, Ghorbangol Ashabi, Maryam Adelipour
Data curation: Amir Hasan Sarkardeh, Ramin Ardalani, Ghorbangol Ashabi, Maryam Adelipour
Formal analysis: Amir Hasan Sarkardeh, Ramin Ardalani, Ghorbangol Ashabi, Maryam Adelipour
Investigation: Amir Hasan Sarkardeh, Ramin Ardalani, Hossein Salehi, Farzaneh Kianian, Elaheh Salmeh
Methodology: Amir Hasan Sarkardeh, Ramin Ardalani, Hossein Salehi, Farzaneh Kianian, Elaheh Salmeh, Amirabbas Rahimi
Project administration: Mina Ranjbaran
Resources: Mina Ranjbaran, Amirabbas Rahimi
Software: Amir Hasan Sarkardeh, Ramin Ardalani, Ghorbangol Ashabi, Maryam Adelipour
Supervision: Mina Ranjbaran
Validation: Ramin Ardalani, Amirabbas Rahimi, Ghorbangol Ashabi, Maryam Adelipour
Writing–original draft: Amir Hasan Sarkardeh, Ramin Ardalani
Writing–review & editing: Mina Ranjbaran, Maryam Adelipour
All authors reviewed and approved the final manuscript.

Funding

This work was supported by Tehran University of Medical Sciences, Tehran, Iran (grant numbers 1402-3-101-68452 and 1402-4-101-69469).

Acknowledgments

The authors thank BioRender for the platform used to prepare the original graphical material. The revised manuscript underwent comprehensive English-language editing for grammar, syntax, terminology, and claim calibration.

Declaration of Generative AI and AI-Assisted Technologies in the Manuscript Preparation Process

During the preparation of this manuscript, the authors used QuillBot to assist with language refinement, grammar, clarity, and paraphrasing of the manuscript text. The authors carefully reviewed and edited all AI-assisted content and take full responsibility for the accuracy, originality, and integrity of the manuscript, including all data, analyses, interpretations, and conclusions.

Competing Interests

The authors declare no competing interests.

Data Availability

Additional datasets are available from the corresponding author on reasonable request.

References

1. Self WK, Holtzman DM. Emerging diagnostics and therapeutics for Alzheimer's disease. Nat Med 2023;29:2187-99. doi: 10.1038/s41591-023-02505-2
2. Seshadri S, Wolf PA. Lifetime risk of stroke and dementia: current concepts, and estimates from the Framingham Study. Lancet Neurol 2007;6(12):1106-14. doi: 10.1016/S1474-4422(07)70291-0
3. Reitz C. Genetic diagnosis and prognosis of Alzheimer's disease: challenges and opportunities. Expert Rev Mol Diagn 2015;15(3):339-48. doi: 10.1586/14737159.2015.1002469
4. Hansson O. Biomarkers for neurodegenerative diseases. Nat Med 2021;27:954-63. doi: 10.1038/s41591-021-01382-x
5. Long JM, Holtzman DM. Alzheimer disease: an update on pathobiology and treatment strategies. Cell 2019;179(2):312-39. doi: 10.1016/j.cell.2019.09.001
6. Hampel H, Vassar R, De Strooper B, Hardy J, Willem M, Singh N, et al. The β-secretase BACE1 in Alzheimer's disease. Biol Psychiatry 2021;89(8):745-56. doi: 10.1016/j.biopsych.2020.02.001
7. Izquierdo P, Jolivet RB, Attwell D, Madry C. Amyloid plaques and normal ageing have differential effects on microglial Ca2+ activity in the mouse brain. Pflugers Arch 2024;476(2):257-70. doi: 10.1007/s00424-023-02871-3
8. Oddo S, Caccamo A, Shepherd JD, Murphy MP, Golde TE, Kayed R, et al. Triple-transgenic model of Alzheimer's disease with plaques and tangles: intracellular Aβ and synaptic dysfunction. Neuron 2003;39(3):409-21. doi: 10.1016/S0896-6273(03)00434-3
9. Steiner H, Haass C. Intramembrane proteolysis by presenilins. Nat Rev Mol Cell Biol 2000;1(3):217-24. doi: 10.1038/35043065
10. Kamatham PT, Shukla R, Khatri DK, Vora LK. Pathogenesis, diagnostics, and therapeutics for Alzheimer's disease: Breaking the memory barrier. Ageing Res Rev 2024;101:102481. doi: 10.1016/j.arr.2024.102481
11. Mackiewicz J, Lisek M, Boczek T. Targeting CaN/NFAT signaling in Alzheimer's brain degeneration. Front Immunol 2023;14:1281882. doi: 10.3389/fimmu.2023.1281882
12. Heneka MT, Carson MJ, El Khoury J, Landreth GE, Brosseron F, Feinstein DL, et al. Neuroinflammation in Alzheimer's disease. Lancet Neurol 2015;14(4):388-405. doi: 10.1016/S1474-4422(15)70016-5
13. Hong S, Beja-Glasser VF, Nfonoyim BM, Frouin A, Li S, Ramakrishnan S, et al. Complement and microglia mediate early synapse loss in Alzheimer mouse models. Science 2016;352(6286):712-6. doi: 10.1126/science.aad8373
14. Lian H, Yang L, Cole A, Sun L, Chiang AC, Fowler SW, et al. NFκB-activated astroglial release of complement C3 compromises neuronal morphology and function associated with Alzheimer's disease. Neuron 2015;85(1):101-15. doi: 10.1016/j.neuron.2014.11.018
15. Stallings NR, Puttaparthi K, Luther CM, Burns DK, Elliott JL. Progressive motor weakness in transgenic mice expressing human TDP-43. Neurobiol Dis 2010;40(2):404-14. doi: 10.1016/j.nbd.2010.06.017
16. Galloway DA, Phillips AEM, Owen DRJ, Moore CS. Phagocytosis in the Brain: Homeostasis and Disease. Front Immunol 2019;10:790. doi: 10.3389/fimmu.2019.00790
17. Capilla-López MD, Deprada A, Andrade-Talavera Y, Martínez-Gallego I, Coatl-Cuaya H, Sotillo P, et al. Synaptic vulnerability to amyloid-β and tau pathologies differentially disrupts emotional and memory neural circuits. Mol Psychiatry 2025;30(7):2966-79. doi: 10.1038/s41380-025-02901-9
18. Solovyev N, Drobyshev E, Bjørklund G, Dubrovskii Y, Lysiuc R, Rayman MP. Selenium, selenoprotein P, and Alzheimer's disease: is there a link? Free Radic Biol Med 2018;127:124-33. doi: 10.1016/j.freeradbiomed.2018.02.030
19. Linker RA, Lee DH, Ryan S, Van Dam AM, Conrad R, Bista P, et al. Fumaric acid esters exert neuroprotective effects in neuroinflammation via activation of the Nrf2 antioxidant pathway. Brain 2011;134(Pt 3):678-92. doi: 10.1093/brain/awq386
20. Schulze-Topphoff U, Varrin-Doyer M, Pekarek K, Spencer CM, Shetty A, Sagan SA, et al. Dimethyl fumarate treatment induces adaptive and innate immune modulation independent of Nrf2. Proc Natl Acad Sci U S A 2016;113(17):4777-82. doi: 10.1073/pnas.1603907113
21. Baird L, Llères D, Swift S, Dinkova-Kostova AT. Regulatory flexibility in the Nrf2-mediated stress response is conferred by conformational cycling of the Keap1-Nrf2 protein complex. Proc Natl Acad Sci U S A 2013;110(38):15259-64. doi: 10.1073/pnas.1305687110
22. Itoh K, Tong KI, Yamamoto M. Molecular mechanism activating Nrf2-Keap1 pathway in regulation of adaptive response to electrophiles. Free Radic Biol Med 2004;36(10):1208-13. doi: 10.1016/j.freeradbiomed.2004.02.075
23. Scuderi SA, Ardizzone A, Paterniti I, Esposito E, Campolo M. Antioxidant and Anti-inflammatory Effect of Nrf2 Inducer Dimethyl Fumarate in Neurodegenerative Diseases. Antioxidants (Basel) 2020;9(7):603. doi: 10.3390/antiox9070630
24. Gold R, Kappos L, Arnold DL, Bar-Or A, Giovannoni G, Selmaj K, et al. Placebo-controlled phase 3 study of oral BG-12 for relapsing multiple sclerosis. N Engl J Med 2012;367(12):1098-107. doi: 10.1056/NEJMoa1114287

25. Sykiotis GP, Bohmann D. Stress-activated cap'n'collar transcription factors in aging and human disease. Sci Signal 2010;3(112):re3. doi: 10.1126/scisignal.3112re3
26. Fonseca-Santos B, Gremião MP, Chorilli M. Nanotechnology-based drug delivery systems for the treatment of Alzheimer's disease. Int J Nanomedicine 2015;10:4981-5003. doi: 10.2147/IJN.S87148
27. Puras G, Mashal M, Zarate J, Agirre M, Ojeda E, Grijalvo S, et al. A novel cationic niosome formulation for gene delivery to the retina. J Control Release 2014;174:27-36. doi: 10.1016/j.jconrel.2013.11.004
28. Ansari M, Eslami H. Preparation and study of the inhibitory effect of nano-niosomes containing essential oil from artemisia absinthium on amyloid fibril formation. Nanomed J 2020;7(3):243-50. doi: 10.22038/nmj.2020.07.0009
29. Ghasemi R, Zarifkar A, Rastegar K, Maghsoudi N, Moosavi M. Repeated intra-hippocampal injection of beta-amyloid 25–35 induces a reproducible impairment of learning and memory: Considering caspase-3 and MAPKs activity. Eur J Pharmacol 2014;726:33-40. doi: 10.1016/j.ejphar.2013.11.034
30. Pan H, Wang Y, Wang X, Yan C. Dimethyl fumarate improves cognitive impairment by enhancing hippocampal brain-derived neurotrophic factor levels in hypothyroid rats. BMC Endocr Disord 2022;22(1):188. doi: 10.1186/s12902-022-01086-4
31. Bernstein KE, Koronyo Y, Salumbides BC, Sheyn J, Pelissier L, Lopes DHJ, et al. Angiotensin-converting enzyme overexpression in myelomonocytes prevents Alzheimer's-like cognitive decline. J Clin Invest 2014;124(3):1000-12. doi: 10.1172/JCI66541
32. Esterbauer H, Cheeseman KH. Determination of aldehydic lipid peroxidation products: malonaldehyde and 4-hydroxynonenal. Methods Enzymol 1990;186:407-21. doi: 10.1016/0076-6879(90)86134-h
33. Azeem A, Anwer MK, Talegaonkar S. Niosomes in sustained and targeted drug delivery: some recent advances. J Drug Target 2009;17(9):671-89. doi: 10.3109/10611860903079454
34. Sethi B, Kumar V, Mahato K, Coulter DW, Mahato RI. Recent advances in drug delivery and targeting to the brain. J Control Release 2022;350:668-87. doi: 10.1016/j.jconrel.2022.08.051
35. Cheignon C, Tomas M, Bonnefont-Rousselot D, Faller P, Hureau C, Collin F. Oxidative stress and the amyloid beta peptide in Alzheimer's disease. Redox Biol 2018;14:450-64. doi: 10.1016/j.redox.2017.10.014
36. Scheltens P, De Strooper B, Kivipelto M, Holstege H, Chételat G, Teunissen CE, et al. Alzheimer's disease. Lancet 2021;397(10284):1577-90. doi: 10.1016/S0140-6736(20)32205-4
37. Brandes MS, Gray NE. NRF2 as a Therapeutic Target in Neurodegenerative Diseases. ASN Neuro 2020;12:1759091419899782. doi: 10.1177/1759091419899782
38. Culbreth M, Aschner M. GSK-3β, a double-edged sword in Nrf2 regulation: implications for neurological dysfunction and disease. F1000Res 2018;7:1043. doi: 10.12688/f1000research.15239.1
39. Liu GH, Qu J, Shen X. NF-κB/p65 antagonizes Nrf2-ARE pathway by depriving CBP from Nrf2 and facilitating recruitment of HDAC3 to MafK. Biochim Biophys Acta 2008;1783(5):713-27. doi: 10.1016/j.bbamcr.2008.01.002
40. Brennan MS, Matos MF, Li B, Hronowski X, Gao B, Juhasz P, et al. Dimethyl fumarate and monoethyl fumarate exhibit differential effects on KEAP1, NRF2 activation, and glutathione depletion in vitro. PLoS One 2015;10(3):e0120254. doi: 10.1371/journal.pone.0120254
41. Unni S, Deshmukh P, Krishnappa G, Kommu P, Padmanabhan B. Structural insights into the multiple binding modes of Dimethyl Fumarate (DMF) and its analogs to the Kelch domain of Keap1. FEBS J 2021;288(5):1599-613. doi: 10.1111/febs.15485
42. Sun E, Motolani A, Campos C, Lu T. The Pivotal Role of NF-κB in the Pathogenesis and Therapeutics of Alzheimer's Disease. Int J Mol Sci 2022;23(16):8972. doi: 10.3390/ijms23168972
43. Abdul HM, Sama MA, Furman JL, Mathis DM, Beckett TL, Weidner AM, et al. Cognitive decline in Alzheimer's disease is associated with selective changes in calcineurin/NFAT signaling. J Neurosci 2009;29(41):12957-69. doi: 10.1523/JNEUROSCI.1064-09.2009
44. Chen CH, Zhou W, Liu S, Deng Y, Cai F, Tone M, et al. Increased NF-κB signalling up-regulates BACE1 expression and its therapeutic potential in Alzheimer's disease. Int J Neuropsychopharmacol 2012;15(1):77-90. doi: 10.1017/S1461145711000149